

# Finite Element Modeling of Airflow During Phonation

P. Šidlof<sup>a,b,\*</sup>, E. Lunéville<sup>c</sup>, C. Chambeyron<sup>c</sup>, O. Doaré<sup>d</sup>, A. Chaigne<sup>d</sup>,  
J. Horáček<sup>b</sup>

<sup>a</sup>Technical University of Liberec, Faculty of Mechatronics, Informatics and Interdisciplinary Studies,  
Studentská 2, 461 17 Liberec 1, Czech Republic

<sup>b</sup>Institute of Thermomechanics, Academy of Sciences of the Czech Republic, Dolejškova 5, 182 00 Praha 8, Czech Republic

<sup>c</sup>École Nationale Supérieure de Techniques Avancées, Unité de Mathématiques Appliquées, 32 Boulevard Victor, 75739 Paris, France

<sup>d</sup>École Nationale Supérieure de Techniques Avancées, Unité de Mécanique, Chemin de la Hunière, 91761 Palaiseau cedex, France

Received 31 August 2009; received in revised form 7 July 2010

---

## Abstract

In the paper a mathematical model of airflow in human vocal folds is presented. The geometry of the glottal channel is based on measurements of excised human larynges. The airflow is modeled by nonstationary incompressible Navier-Stokes equations in a 2D computational domain, which is deformed in time due to vocal fold vibration. The paper presents numerical results and focuses on flow separation in glottis. Quantitative data from numerical simulations are compared to results of measurements by Particle Image Velocimetry (PIV), performed on a scaled self-oscillating physical model of vocal folds.

© 2010 University of West Bohemia. All rights reserved.

*Keywords:* vocal folds, airflow, numerical modeling, ALE, flow separation

---

## 1. Introduction

Human voice is created by passage of airflow between vocal folds, which are located in the upper part of larynx. The physiology of the vocal folds is complex; a thorough anatomic and functional information comprehensible to an engineer can be found e.g. in the monograph of Titze [23]. Basically, the vocal folds (formerly called vocal cords) are two symmetric soft tissue structures fixed between the thyroid and arytenoid cartilages. They are composed of the thyroarytenoid muscle and ligament covered by mucosa.

When air is expired from lungs, the constriction formed by the vocal folds (which is called *glottis*) induces acceleration of the flow. Under certain circumstances (subglottal pressure, glottal width, longitudinal tension in the thyroarytenoid and ligament), fluid-structure interaction between the elastic structure and airflow may invoke vocal fold oscillations. It is important that the vibration is a passive process – when voicing, no sort of periodic muscle contraction is performed.

In mathematical modeling of vocal fold vibration, a classical approach is to reduce the mechanical part of the problem into a small system of rigid masses, springs and dampers, which is further coupled to a simplified flow model (see e.g. the fundamental work of Ishizaka & Flanagan from 1972 [10], or for example the models of Titze or Pelorson [22, 16]). The models often comprise semiempirical relations and constants. Although these lumped-parameter models are still widely used and can provide useful and computationally inexpensive data in specific cases,

---

\*Corresponding author. Tel.: +420 485 353 015, e-mail: sidlof@it.cas.cz.

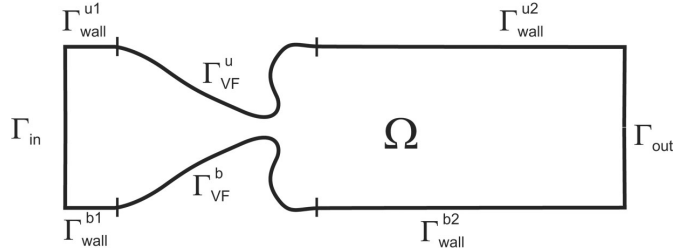


Fig. 1. Sketch of the computational domain and definition of its boundary parts

some more complex techniques have also been employed in recent years [21, 5, 28]. These are related mainly to the boom of finite element and finite volume codes, which allow realistic modeling both of the flow and of the elastic deformations.

Within this paper, a finite element model of airflow through vibrating vocal folds is described. The model enables to study the development of pressure and velocity fields along the vibrating vocal folds, observe the behavior of the pulsating glottal jet and vortex dynamics downstream glottis. In particular, the mathematical model is used to assess flow separation in glottis – a phenomenon, which is not yet fully understood, even though it is of high importance and interest for vocal fold researchers. The numerical results are compared with experimental data, obtained on a physical self-oscillating vocal fold model by means of Particle Image Velocimetry (PIV) measurements.

## 2. Methods

### 2.1. Mathematical model

In the first approximation, it can be assumed that the flow field in the glottal region does not change significantly along the anterior-posterior axis. Thus, it seems reasonable to investigate only 2D flow fields in the coronal plane. In the mathematical model, this approach facilitates substantially the numerical computation: the 3D and 2D models do not differ in principle, but the latter requires much less computational power. The Mach numbers encountered in phonation are rather low (in the order of magnitude,  $Ma = 0.1$ ). This allows to model the flow as incompressible. In the works on phonatory airflow, there has been controversy whether the viscous effects play an important role or not. In the model presented here, viscosity was taken into account.

In the following, we are going to describe the flow of an incompressible viscous Newtonian fluid in a bounded 2D domain. Let  $\Omega_t \subset \mathbb{R}^2$  be the domain occupied by the fluid (the subscript ‘ $t$ ’ is used to denote the time-variable domains). The boundary  $\Gamma_t = \partial\Omega_t$  is composed of four non-intersecting parts (see Fig. 1):

$$\Gamma_t = \Gamma_{in} \cup \Gamma_{out} \cup \Gamma_{wall} \cup \Gamma_{VF,t}, \quad (1)$$

where  $\Gamma_{in}$  and  $\Gamma_{out}$  are virtual boundaries representing the inlet and outlet,  $\Gamma_{wall} = \Gamma_{wall}^{b1} \cup \Gamma_{wall}^{b2} \cup \Gamma_{wall}^{u1} \cup \Gamma_{wall}^{u2}$  is the fixed wall, which is not a function of time, and  $\Gamma_{VF,t} = \Gamma_{VF,t}^b \cup \Gamma_{VF,t}^u$  stands for the surface of the moving vocal folds. The superscripts ‘ $b$ ’ and ‘ $u$ ’ denote the bottom and upper parts, respectively.

The flow is modeled by incompressible non-stationary Navier-Stokes equations in 2D, which are numerically solved by the finite element method (FEM). The main complication

is that due to vocal fold vibration, the computational domain  $\Omega_t$  changes in time (which implies that the mesh is deformed, too); this would make the straightforward FE discretization inconvenient. Therefore the equations are reformulated using arbitrary Lagrangian-Eulerian (ALE) approach [15]. The ALE-form of the Navier-Stokes equations reads

$$\begin{aligned} \frac{D^A}{Dt} \mathbf{u} + [(\mathbf{u} - \mathbf{w}) \cdot \nabla] \mathbf{u} + \nabla p - \nu \Delta \mathbf{u} &= 0 & \text{in } \Omega_t \\ \operatorname{div} \mathbf{u} &= 0 & \text{in } \Omega_t \end{aligned} \quad (2)$$

where  $\mathbf{u}$  is flow velocity,  $p$  stands for kinematic pressure,  $\nu$  is kinematic viscosity. The vector  $\mathbf{w}$  denotes the *domain velocity* (velocity of the meshpoints) and  $\frac{D^A}{Dt}$  is so-called *ALE-derivative*, which can be easily discretized even in time-dependent computational domains.

Setting the boundary conditions represents a rather delicate question. On the outlet  $\Gamma_{out}$ , a common choice is the “do-nothing condition” [24]

$$\begin{aligned} -\nu \frac{\partial \mathbf{u}}{\partial \mathbf{n}}(t, \mathbf{x}) + p(t, \mathbf{x}) \mathbf{n}(\mathbf{x}) &= p_{ref} \mathbf{n}(\mathbf{x}) \\ \text{for } \mathbf{x} \in \Gamma_{out}, t \in [0, T] \end{aligned} \quad (3)$$

where  $\partial/\partial \mathbf{n}$  denotes the normal derivative,  $\mathbf{n}(\mathbf{x})$  is the unit outer normal to  $\Gamma_{out}$  and  $p_{ref}$  is a reference pressure. In certain cases, however, this condition becomes too vague – it allows the flow returning to the domain  $\Omega_t$  through  $\Gamma_{out}$  (e.g. when a large vortex arrives to  $\Gamma_{out}$ ). Thus, the total influx into the domain  $\Omega_t$  can grow infinite and the numerical scheme tends to diverge. To suppress this inconvenience, the boundary condition (3) can be modified during the derivation of the weak form of the equations.

On the inlet  $\Gamma_{in}$ , two conditions were tested: either a parabolic profile of the vertical velocity component, or the (modified) do-nothing condition as on  $\Gamma_{out}$ . The difference  $p_{ref}^{in} - p_{ref}^{out}$  then represents the transglottal pressure (approximately equal to the lung pressure during phonation), which drives the flow.

Since we use a viscous model, the “no-slip condition”

$$\mathbf{u}(t, \mathbf{x}) = \mathbf{0} \quad \text{for } \mathbf{x} \in \Gamma_{wall}, t \in [0, T] \quad (4)$$

is prescribed on the fixed walls  $\Gamma_{wall}$ . On the moving vocal fold surfaces, the velocity of the fluid particles must be equal to the velocity of the moving surface, which is given by the domain velocity  $\mathbf{w}$ .

For the structural part of the problem, the real, continuously elastic vocal fold was modeled by a rigid body supported by two springs and dampers (similarly as in previous work [9]). The kinematic model reflects two basic modes of the vocal fold motion: vertical shift and rocking. It is not difficult to derive the equations of motion of the system in a standard form

$$\mathbb{M} \ddot{\mathbf{q}} + \mathbb{B} \dot{\mathbf{q}} + \mathbb{K} \mathbf{q} = \mathbf{F} \quad (5)$$

where  $\mathbb{M}$ ,  $\mathbb{B}$ ,  $\mathbb{K}$  are the mass, damping and stiffness matrices,  $\mathbf{q}$  denotes the vector of generalized coordinates (shift and rotation) and  $\mathbf{F} = (F_f, M_f)^T$  stands for the vector of generalized forces (vertical force and momentum), induced on the boundary  $\Gamma_{VF,t}$  by the flow.

The full coupled problem can be solved in the following procedure: Assuming that the solution of the Navier-Stokes equations (2) on a specific time level  $t$  and domain  $\Omega_t$  is known,

the total vertical force  $F_f$  and momentum  $M_f$ , by which the fluid acts on the vocal fold, is given by the integration of the stress vector  $\boldsymbol{\tau}$  over the surface of the moving vocal fold:

$$F_f = \int_{\Gamma_{VF,t}^b} \tau_2 \, d\sigma = \int_{\Gamma_{VF,t}^b} \sum_{j=1}^2 \mathbb{T}_{2j} n_j \, d\sigma, \quad (6)$$

$$M_f = \int_{\Gamma_{VF,t}^b} \sum_{l=1}^2 \left( \mathbb{T}_{1l} n_l x_2 - \mathbb{T}_{2l} n_l x_1 \right) d\sigma. \quad (7)$$

Here  $\mathbb{T}$  is the stress tensor and  $\mathbf{n}$  the unit outer normal to the vocal fold surface. The stress tensor  $\mathbb{T}$  is calculated from the pressure and velocity fields  $p(t, x)$  and  $\mathbf{u}(t, x)$  on time level  $t$  according to the constitutive relation valid for Newtonian fluids.

Once the excitation forces are known, it is possible to proceed to the next time level  $t + \tau$  by performing one step of the Runge-Kutta method in the time-discretized equations of motion. This yields new coordinates of the structure, which uniquely determine the shape of the domain  $\Omega_{t+\tau}$ . With the knowledge of the solution from the previous two time levels, the Navier-Stokes equations can be numerically solved on the new time level  $t + \tau$  and new domain  $\Omega_{t+\tau}$  using the finite element method.

## 2.2. Discretization and numerical solution

The finite element method, which is widely used for numerical solution of elliptic and parabolic partial differential equations for instance in structural mechanics, seems to be somewhat less popular in computational fluid dynamics (CFD); actually most of the commercial CFD codes employ some variant of the finite volume method. This is caused by the computational costs of the FEM (with the same number of mesh elements, lower-order methods – such as the finite volume method – offer less accurate, but less computationally expensive solutions), but also by the fact, that for high Reynolds numbers the standard finite element method does not give reliable results. To understand this unfavorable feature, it is necessary to realize that for high-velocity flows the viscous term in the Navier-Stokes equations becomes insignificant against the convective term. It is well known that for such systems with dominating convection (sometimes also called singularly perturbed problems), standard finite element method is not suitable as it produces nonphysical, “spurious” oscillations in the solution [8]. There exist several stabilization concepts, which can help overcome this numerical problem, namely streamline diffusion method (alias streamline upwind Petrov-Galerkin method, SUPG), Galerkin least-squares method or residual-based stabilizations [12]. These methods, however, require a very careful choice of the stabilization parameters. Since the Reynolds numbers of typical glottal flows do not usually exceed values of  $\text{Re} = 1\,000 - 5\,000$ , the standard, non-stabilized finite element numerical scheme was used in this study.

For the numerical solution of the Navier-Stokes equations using FEM, these need first to be semidiscretized in time. Let us define the discrete time level  $t_i = i \tau$ , where  $\tau$  is a constant timestep, and the approximate flow velocity, pressure and domain velocity on this time level

$$\mathbf{u}^i(\mathbf{x}) \approx \mathbf{u}(t_i, \mathbf{x}), p^i(x) \approx p(t_i, \mathbf{x}), \mathbf{w}^i(x) \approx \mathbf{w}(t_i, \mathbf{x}), \mathbf{x} \in \Omega_{t_i}. \quad (8)$$

Using a second-order backward difference in time for the ALE-derivative, we get the semi-discrete Navier-Stokes equations for the functions  $\mathbf{u}^{n+1} : \Omega_{t_{n+1}} \mapsto \mathbb{R}^2$  and  $p^{n+1} : \Omega_{t_{n+1}} \mapsto \mathbb{R}$

$$\frac{3 \mathbf{u}^{n+1}}{2 \tau} + [(\mathbf{u}^{n+1} - \mathbf{w}^{n+1}) \cdot \nabla] \mathbf{u}^{n+1} + \nabla p^{n+1} - \nu \Delta \mathbf{u}^{n+1} = \frac{4 \hat{\mathbf{u}}^n - \hat{\mathbf{u}}^{n-1}}{2 \tau}$$

$$\operatorname{div} \mathbf{u}^{n+1} = 0, \quad (9)$$

where  $\hat{\mathbf{u}}^i(\mathbf{x}^{n+1}) = \mathbf{u}^i(A_{t_i}(A_{t_{n+1}}^{-1}(\mathbf{x}_{n+1})))$  and  $A_{t_i}$  is the ALE-mapping of the undeformed, “reference” domain  $\Omega_0$  onto the current, deformed domain  $\Omega_{t_i}$ .

Due to the presence of the nonlinear, convective term  $[(\mathbf{u}^{n+1} - \mathbf{w}^{n+1}) \cdot \nabla] \mathbf{u}^{n+1}$  in the Navier-Stokes equations (9), the system cannot be solved in a straightforward way. Instead, it is first necessary to linearize the equations, i.e. to replace the first occurrence of the sought velocity vector  $\mathbf{u}^{n+1}$  by some vector  $\mathbf{u}^*$ , which is already known:

$$[(\mathbf{u}^{n+1} - \mathbf{w}^{n+1}) \cdot \nabla] \mathbf{u}^{n+1} \approx [(\mathbf{u}^* - \mathbf{w}^{n+1}) \cdot \nabla] \mathbf{u}^{n+1}. \quad (10)$$

For quasisteady flows it is possible to use the solution from the previous timestep  $\mathbf{u}^n$ . To increase precision for the non-stationary flow it is better to employ an iteration process, using  $\mathbf{u}^n$  as the first iteration.

To simplify the equations, let us further denote  $\mathbf{u} \equiv \mathbf{u}^{n+1}$ ,  $\mathbf{w} \equiv \mathbf{w}^{n+1}$ ,  $p \equiv p^{n+1}$ ,  $\Omega \equiv \Omega_{t_{n+1}}$  and  $\Gamma_{VF} \equiv \Gamma_{VF, t_{n+1}}$ . The starting point for the finite element discretization of any system of partial differential equations is its weak (variational) form. It is obtained by multiplying the classical form (9) by an arbitrary test function from the relevant functional space (see [8] for details) and integrating over  $\Omega$ :

$$\frac{3}{2\tau} \int_{\Omega} \mathbf{u} \cdot \mathbf{v} \, d\mathbf{x} + \int_{\Omega} \left( [(\mathbf{u}^* - \mathbf{w}) \cdot \nabla] \mathbf{u} \right) \cdot \mathbf{v} \, d\mathbf{x} + \int_{\Omega} \nabla p \cdot \mathbf{v} \, d\mathbf{x} - \int_{\Omega} \nu \Delta \mathbf{u} \cdot \mathbf{v} \, d\mathbf{x} = \frac{1}{2\tau} \int_{\Omega} (4\hat{\mathbf{u}}^n - \hat{\mathbf{u}}^{n-1}) \cdot \mathbf{v} \, d\mathbf{x} \quad \forall \mathbf{v} \in \mathbf{W}, \quad (11)$$

$$\int_{\Omega} q \operatorname{div} \mathbf{u} \, d\mathbf{x} = 0 \quad \forall q \in Q. \quad (12)$$

In our case, the pressure solution is from the space of square-integrable functions  $p \in L^2(\Omega)$ , the velocity solution will be sought in the Sobolev space  $\mathbf{u} \in \mathbf{Y} = (H^1(\Omega))^2$ , and the velocity and pressure test function spaces  $\mathbf{W}$  and  $Q$  are defined as follows:

$$\mathbf{W} = \{ \mathbf{v} \in \mathbf{Y} : \mathbf{v}|_{\Gamma_{in} \cup \Gamma_{wall} \cup \Gamma_{VF}} = 0 \} \quad (13)$$

$$Q = L^2(\Omega). \quad (14)$$

Using Green’s theorem, the boundary conditions and the properties of the test functions (see [18] for details), we get the ultimate form of the weak semidiscretized ALE Navier-Stokes equations:

$$\begin{aligned} & \frac{3}{2\tau} \int_{\Omega} \mathbf{u} \cdot \mathbf{v} \, d\mathbf{x} + \nu \int_{\Omega} \nabla \mathbf{u} \cdot \nabla \mathbf{v} \, d\mathbf{x} - \int_{\Omega} p \operatorname{div} \mathbf{v} \, d\mathbf{x} + \frac{1}{2} \int_{\Omega} \left( [(\mathbf{u}^* - 2\mathbf{w}) \cdot \nabla] \mathbf{u} \right) \cdot \mathbf{v} \, d\mathbf{x} \\ & \quad - \frac{1}{2} \int_{\Omega} \left( [\mathbf{u}^* \cdot \nabla] \mathbf{v} \right) \cdot \mathbf{u} \, d\mathbf{x} + \frac{1}{2} \int_{\Gamma_{out}} (\mathbf{u}^* \cdot \mathbf{n})^+ \mathbf{u} \cdot \mathbf{v} \, d\mathbf{x} = \\ & = \frac{1}{2\tau} \int_{\Omega} (4\hat{\mathbf{u}}^n - \hat{\mathbf{u}}^{n-1}) \cdot \mathbf{v} \, d\mathbf{x} - \int_{\Gamma_{out}} p_{ref} \mathbf{v} \cdot \mathbf{n} \, d\sigma \quad \forall \mathbf{v} \in \mathbf{W}, \end{aligned} \quad (15)$$

$$\int_{\Omega} q \operatorname{div} \mathbf{u} \, d\mathbf{x} = 0 \quad \forall q \in Q, \quad (16)$$

where  $(\mathbf{u}^* \cdot \mathbf{n})^+$  denotes the positive part of the scalar product introduced to stabilize the outflow boundary condition.

The weak Navier-Stokes equations (15,16) were discretized in space using standard Galerkin finite element method on a triangular mesh with Taylor-Hood  $P^2/P^1$  (quadratic for velocity, linear for pressure) or  $P^3/P^2$  (cubic for velocity, quadratic for pressure) elements. The mesh was refined near glottis in order to resolve better for large gradients in the solution and for flow separation downstream glottis.

The numerical solution of the discretized problem was implemented using an open-source library *Mélina* [14]. For the solution of the resulting linear system (with typically 200 000 degrees of freedom), a direct linear solver *UMFPack* [4] was used. This package, which is used as a default sparse matrix solver in recent versions of *Matlab*, uses a direct multifrontal method, suitable for generally nonsymmetric sparse matrices. Its performance may be boosted by installation of a suitable BLAS (Basic Linear Algebra Subsystem). On Intel processors, the overall performance of the binary code can be further improved by compiling the libraries and the program source code with Intel Fortran Compiler (instead of GNU Fortran compiler, such as *f77* or *gfortran*), and by setting appropriate optimization flags.

### *2.3. Geometry of the glottal channel*

The vocal fold geometry plays a crucial role in phonation. The vocal fold shape is directly related to the mass distribution in the vibrating elastic element, which influences strongly the vibration eigenmodes [2]. Besides, vocal folds constitute the channel profile and thus their shape has a dramatic impact on glottal aerodynamics – a small variation of the vocal fold shape or position may change the flow regime and the resulting aerodynamic forces, which excite the system [21, 25]. However, quantitative information on the phonatory shape of human vocal folds has been scarce. Accurate data are lacking especially on the coronal cross-sectional shape of the vocal folds.

Many of the current vocal fold models (both mathematical and physical) use the geometry specified originally by Scherer [17]. The major advantage of this so-called M5 shape is that it is simple and easily parametrizable. However, it seems to be based on somewhat arbitrary information, not on precise anatomic data. The geometry of the mathematical model presented in this paper, i.e. the 2D shape of the vocal folds and adjoining vocal tract, was specified according to measurements on excised human larynges. Details can be found in [20].

### *2.4. Physical model of vocal folds*

To validate the results from the mathematical model, a self-oscillating physical model of vocal folds was fabricated at ENSTA Paris. Detailed description of this model and results of the measurements can be found e.g. in [18, 19]. Let us just say here that it was designed as a vocal-fold-shaped element vibrating in the wall of a rectangular wind tunnel. The model is 4 : 1 scaled; to avoid difficulties with asymmetric vocal fold vibration, one of the vocal folds is static. Best possible effort was made to keep the important dimensionless parameters (Reynolds and Strouhal numbers) of the model close to the real situation. The shape of the vocal folds was specified in the same fashion as in the mathematical model.

The experimental setup was equipped with a PIV system (*Dantec – New Wave Research Solo III*) for measuring airflow velocity fields, an ultrasonic flowmeter (*GE Panametric GC 868*) measuring the flow rate, and two *B&K 4507C* accelerometers fixed under the vibrating vocal fold used to record mechanical vibration. The acoustic data were measured by dynamic pressure transducers (*Validyne DP15TL*) and measuring microphones (*G.R.A.S. 1/8" type 2692*).

### 3. Results

The numerical model was used to perform a series of computations for a broad range of parameters, representing various types of phonation. Here we will demonstrate results of one specific numerical simulation, whose parameters were set to match the vibration pattern of one of the most stable modes of the physical model: forced 2DOF vibration with frequency  $f = 10.9$  Hz (corresponding to about  $f = 90$  Hz in lifesize), periodic oscillation with an amplitude of about 1.5 mm without vocal fold collisions (modeling breathy phonation or whispering) and transglottal pressure  $\Delta p = 45$  Pa (180 Pa in lifesize). The computational mesh was triangular and consisted of 16537  $P^3/P^2$  (bicubic for velocity, parabolic for pressure) elements. The nonstabilized finite element scheme implemented on this mesh allows to reach Reynolds numbers of about 5 000, which is sufficient to model the values observed in human vocal folds. Timestep of the numerical simulation was set to  $\tau = 0.5$  ms.

Fig. 2 demonstrates the calculated velocity fields for these parameters at four time instants of one vocal fold oscillation cycle. We see that the airflow separates from the vocal fold wall shortly downstream the narrowest cross-section and forms a jet. The vortices, which shed from the shear layer of the jet, propagate slowly downstream and interact with the jet and among themselves. Instead of remaining symmetric with regard to the channel axis, the jet tends to adhere to one of the vocal fold surfaces by Coanda effect. This effect occurs very distinctly when the glottis closes. The glottal jet skews from the straight direction when glottis is widely open, too, but in this case it does so rather due to interaction with vortex structures downstream glottis.

The flow velocity fields calculated by the numerical code can be directly compared to results of PIV measurements on the physical model. However, it is necessary to realize that we handle 2D vector data from an inherently nonstationary process. Thus, it is nearly always possible to find time instants where the results appear to match well, but also those where the velocity fields look different. Objectively, it can be stated that the result of the numerical simulation shown in Fig. 2 matches with the experimental results in terms of maximum jet velocity ( $u_{max} = 12$  m/s in numerical results,  $u_{max} = 11$  m/s in PIV measurements) and general flow structure.

Unlike the global, time-developing velocity fields, there are certain features of the glottal flow which may be extracted from the results and compared directly. One of them, which is of high interest for vocal fold researchers, is the position of the flow separation point, which was identified and processed from both numerical and experimental results.

In many simplified models of airflow in vocal folds, the position of the separation point is either fixed to the superior margin of the vocal folds [26, 27] or supposed to move along the divergent part of glottis. In the latter case, its position is usually specified using a semiempirical criterion, which states that the jet separates at the position where the channel cross-section  $A$  reaches

$$A/A_{min} = FSR, \quad (17)$$

where  $A_{min}$  is the minimum glottal cross-section and  $FSR$  so-called “flow separation ratio”. In numerous published papers, the ratio is assumed to remain constant during vocal fold oscillation cycle, and various values of  $FSR$  are proposed: Deverge et al. [6] sets  $FSR = 1.2$  (based on the pioneer work of Pelorson [16] and private communication with Liljencrants), Lucero et al. [13] uses  $FSR = 1.1$ . In their comparative study, Decker [5] tested different values of the flow separation ratio:  $FSR = 1.2$  and  $FSR = 1.47$  (according to finite volume computations of Alipour [1]). Recently, Cisonni [3] published data on flow separation point ratio computed by inverse simplified flow models.

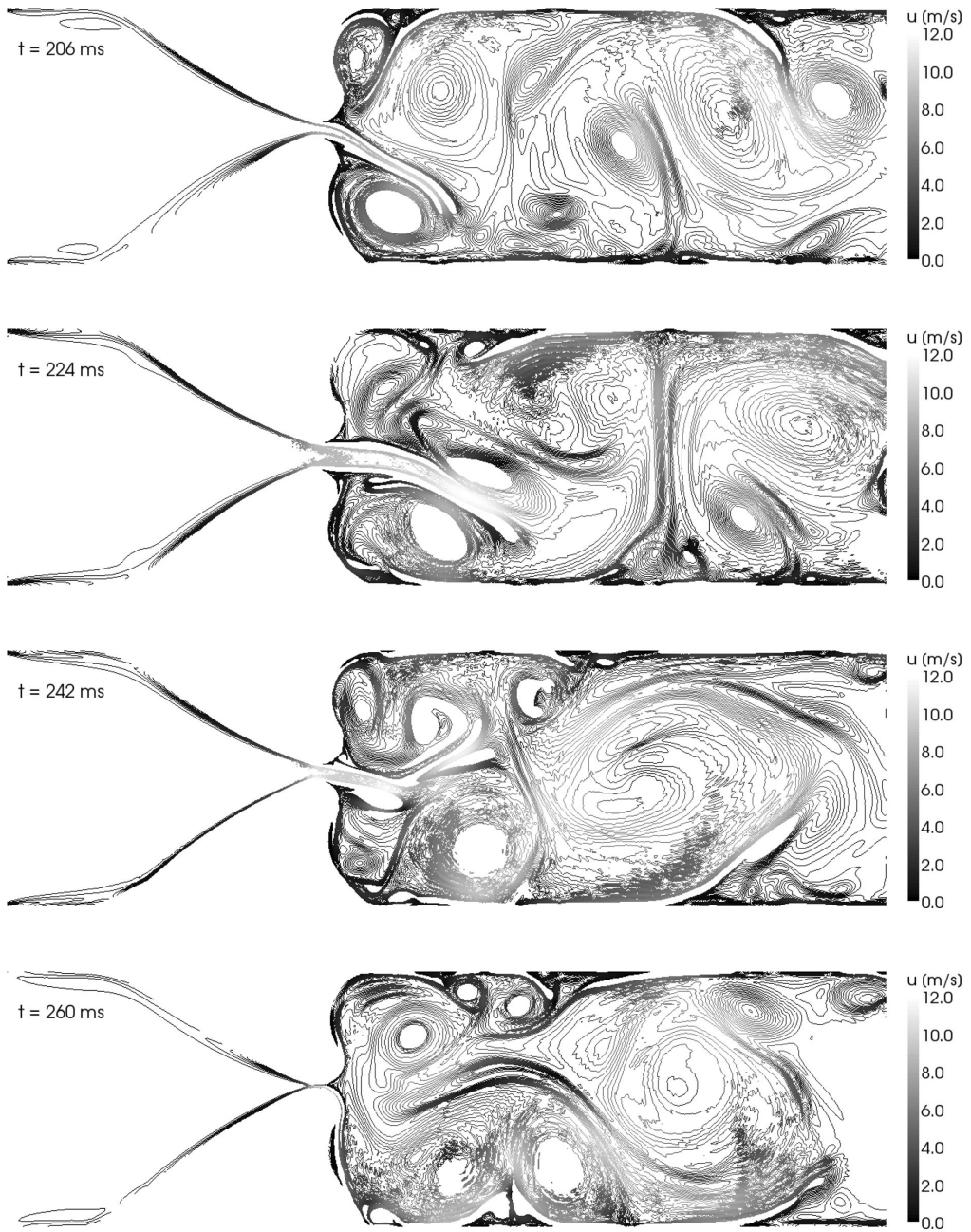


Fig. 2. Velocity fields in glottis in four phases of one vocal fold vibration cycle. Half of the opening phase ( $t = 206$  ms), fully open glottis ( $t = 224$  ms), middle of the closing phase ( $t = 242$  ms), maximum vocal fold closure ( $t = 260$  ms). Vorticity contours colored by velocity magnitude)

All the works mentioned so far implicitly assume that the flow field is symmetric. Since this is rarely the case in real vocal folds, it seems adequate to measure the flow separation ratio from the channel axis and define it independently for upper and lower vocal fold. If we consider that in real physiology, the vocal channel is not horizontal but vertical, and call these “left” and “right” flow separation ratio, we may plot them in time and compare how do they behave in the computational and physical models.

Fig. 3 shows the computational and experimental results for the left separation ratio FSR-L. During most of the oscillation cycle, the ratio remains between 1.1–1.3, which is in good agreement with the values mentioned in previous paragraph. The experimental data are more scattered mostly due to lower resolution of the measured velocity fields. However, when vocal folds come close each other (i.e. near the dashed line denoting beginning of the opening phase, and at the right side of the plot near end of the closing phase), the ratio increases. The same, even much more prominent behavior, can be seen in Fig. 4 for FSR-R. In principle, this quantifies what has been stated before – near glottal closure the jet tends to adhere to one of the vocal folds (right one, in this case).

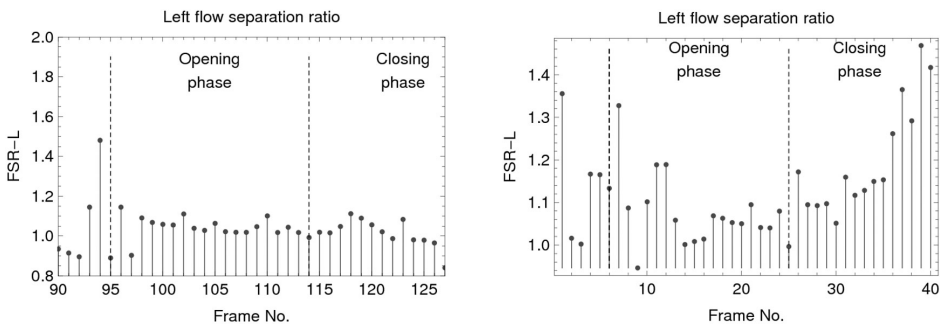


Fig. 3. Left flow separation ratio – computational (left) and experimental (right)

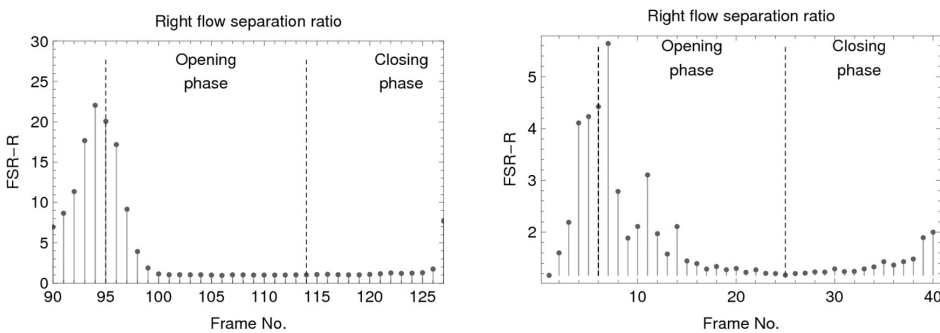


Fig. 4. Right flow separation ratio – computational (left) and experimental (right)

To demonstrate how the flow separation behaves in overall, it is possible to plot the glottal orifice width together with the position of the flow separation point for both sides together (see Fig. 5). The plot shows four periods of oscillation. Apparently the jet inclines rather to the right side. Even though the flow separation process is not perfectly periodic (also due to interaction of the jet with stochastic turbulent structures downstream glottis), it is obvious that from the perspective of flow separation, important matters occur when the vocal folds get close together.

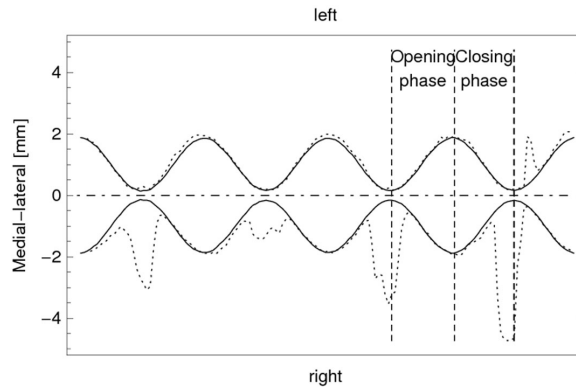


Fig. 5. Glottis opening (solid line) and position of the flow separation point (dotted line) in four vocal fold oscillation cycles. Computational results

#### 4. Conclusion

A new, finite element model of phonatory airflow was developed. The computational results compare well with the experimental data obtained from a physical vocal fold model in terms of maximum glottal jet velocity, location of major vortex structures and overall flow dynamics, and seem to correspond when compared visually. However, it should be noted that the flow is neither stationary nor perfectly periodical, and thus such comparison of the flow patterns might be somewhat subjective.

There are some aspects, which restrict the class of vocal fold regimes possible to model computationally – the main limitation is currently the fact that within the mathematical model, the vocal folds are not allowed to collide. The processes accompanying glottal closure are complex and from the algorithmic point of view, the separation of the computational domain into two, necessity to introduce additional boundary conditions and to handle pressure discontinuity when reconnecting the domains represent a very complicated problem. Yet it will be necessary to deal with this task in future, if the mathematical model should be employed to model regular loud human phonation.

The next problem which arises is that the vortex dynamics in 2D and 3D are different. In 2D, the primary mechanism of vortex vanishing is viscous dissipation. In 3D reality, on the other hand, the original single vortex tube might disintegrate into several smaller vortices, which mutually interact and tend to align their axes with the flow direction. As a result, in a 2D section the vortices seem to dissipate and disappear faster. Consequently, results of a 2D simulation may be reliable near glottis, which has a strong effect of bi-dimensionalizing the airflow, but must be judged carefully further downstream.

The model was also used to assess and quantify flow separation in glottis. Both numerical and experimental results suggest that the usage of the classical flow separation criterion with values ranging from 1.1 to 1.3 seems to be quite plausible for the most of the vocal fold oscillation cycle, where the vocal folds are not too close together. Near glottal closure, however, the airflow separates much further downstream since it tends to adhere to one of the vocal folds.

Although more experimental data with higher resolution would be needed to draw more systematic and definitive conclusions, we believe that the results presented here give new insight into the problematic of flow separation during human phonation.

## Acknowledgements

The research has been financially supported by the Grant Agency of the Academy of Sciences of the Czech Republic, project No. KJB200760801 *Mathematical modeling and experimental investigation of fluid-structure interaction in human vocal folds*, research plan no. AV0Z20760514. Let us also acknowledge the support of UME ENSTA Paris, who provided the experimental background.

## References

- [1] Alipour, F., Scherer, R., Flow separation in a computational oscillating vocal fold model, *Journal of the Acoustical society of America* 116 (3) (2004), 1 710–1 719.
- [2] Berry, D. A., Mechanism of modal and non-modal phonation, *Journal of Phonetics* 29 (2001), 431–450.
- [3] Cisonni, J., Van Hirtum, A., Pelorson, X., Willems, J., Theoretical simulation and experimental validation of inverse quasi-one-dimensional steady and unsteady glottal flow models, *Journal of the Acoustical society of America* 124 (1) (2008), 535–545.
- [4] Davis, T. A., UMFPack: unsymmetric multifrontal sparse LU factorization package, University of Florida, Gainesville, FL, USA. <http://www.cise.ufl.edu/research/sparse/umfpack/>.
- [5] Decker, G. Thomson, S., Computational simulations of vocal fold vibration: Bernoulli versus navier-stokes, *Journal of Voice* 21 (3) (2007), 273–284.
- [6] Deverge, M., Pelorson, X., Vilain, C., Lagree, P., Chentouf, F., Willems, J., Hirschberg, A., Influence of collision on the flow through in-vitro rigid models of the vocal folds. *Journal of the Acoustical Society of America* 114(2003), 3 354–3 362.
- [7] Erath, B., Plesniak, M., The occurrence of the coanda effect in pulsatile flow through static models of the human vocal folds. *Experiments in Fluids* (41) (2006), 735–748.
- [8] Feistauer, M., Felcman, J., Straškraba, I., *Mathematical and computational methods for compressible flow*, Clarendon Press, Oxford, 2003.
- [9] Horáček, J., Šidlof, P., Švec, J. G., Numerical simulation of self-oscillations of human vocal folds with Hertz model of impact forces, *Journal of Fluids and Structures* 20 (2005), 853–869.
- [10] Ishizaka, K., Flanagan, J., Synthesis of voiced sounds from a two-mass model of the vocal cords. *The Bell System Technical Journal* 51 (1972), 1 233–1 268.
- [11] Kob, M., Krämer, S., Prévot, A., Triep, M., Brücker, C., 2005, Acoustic measurement of periodic noise generation in a hydrodynamical vocal fold model, *Proceedings of Forum Acusticum, Budapest, 2005*, pp. 2 731–2 736.
- [12] Link, G., *A Finite Element Scheme for Fluid-Solid-Acoustics Interactions and its Application to Human Phonation*, Ph.D. thesis, Der Technischen Fakultät der Universität Erlangen-Nürnberg, Erlangen, 2008.
- [13] Lucero, J., Optimal glottal configuration for ease of phonation, *Journal of Voice* 12 (2) (1998), 151–158.
- [14] Martin, D., *Finite element library Mélina*, Université de Rennes, <http://perso.univ-rennes1.fr/daniel.martin/melina/>.
- [15] Nomura, T., Hughes, T. J., An arbitrary Lagrangian-Eulerian finite element method for interaction of fluid and a rigid body, *Computer methods in applied mechanics and engineering* 95 (1992), 115–138.
- [16] Pelorson, X., Hirschberg, A., van Hassel, R., Wijnands, A., Theoretical and experimental study of quasisteady flow separation within the glottis during phonation. Application to a modified two-mass model, *Journal of the Acoustical Society of America* 96 (6) (1994), 3 416–3 431.

- [17] Scherer, R. C., Shinwari, D., De Witt, K. J., Zhang, C., Kucinski, B. R., Afjeh, A. A., Intraglottal pressure profiles for a symmetric and oblique glottis with a divergence angle of 10 degrees, *Journal of the Acoustical Society of America* 109 (4) (2001), 1 616–1 630.
- [18] Šidlof, P., Fluid-structure interaction in human vocal folds, Ph.D. thesis, Charles University in Prague, 2007.
- [19] Šidlof, P., Doaré, O., Cadot, O., Chaigne, A., Horáček, J., Finite element modeling of airflow in vibrating vocal folds, *Proceedings of International Conference on Voice Physiology and Biomechanics – ICVPB, Tampere, 2008*.
- [20] Šidlof, P., Švec, J. G., Horáček, J., Veselý, J., Klepáček, I., Havlík, R., Geometry of human vocal folds and glottal channel for mathematical and biomechanical modeling of voice production, *Journal of Biomechanics* 41 (2008), 985–995.
- [21] Thomson, S. L., Mongeau, L., Frankel, S. H., Aerodynamic transfer of energy to the vocal folds. *Journal of the Acoustical Society of America* 113 (2005), 1 689–1 700.
- [22] Titze, I. R., The human vocal cords: A mathematical model, Part II, *Phonetica* 29 (1974).
- [23] Titze, I. R., *Principles of Voice Production*, National Center for Voice and Speech, Denver, 2000.
- [24] Turek, S., *Efficient solvers for incompressible flow problems: An algorithmic and computational approach*, Springer-Verlag, Berlin, 1999.
- [25] Vilain, C. E., Pelorson, X., Fraysse, C., Deverge, M., Hirschberg, A., Willems, J., Experimental validation of a quasi-steady theory for the flow through the glottis. *Journal of Sound and Vibration* 276 (2004), 475–490.
- [26] Zanartu, M., Mongeau, L., Wodicka, G., Influence of acoustic loading on an effective single mass model of the vocal folds, *Journal of the Acoustical Society of America* 121 (2) (2007), 1 119–1 129.
- [27] Zhang, Z., Neubauer, J., Berry, D., Physical mechanisms of phonation onset: a linear stability analysis of an aeroelastic continuum model of phonation, *Journal of the Acoustical Society of America* 122 (4) (2007), 2 279–2 295.
- [28] Zörner, S., Numerical study of the human phonation process by the Finite Element Method, *Proceedings of the International Conference on Acoustics NAG/DAGA, Rotterdam, 2009*, 1 718–1 721.